In-plane anisotropy in spin-excitation spectra originating from chain states in $YBa_2Cu_3O_{6+y}$

Tanmoy Das
Theoretical Division, Los Alamos National Laboratory, Los Alamos, New Mexico 87545 USA
(Dated: March 22, 2012)

We present a random-phase approximation (RPA)-based multilayer spin-susceptibility calculation for the trilayer $YBa_2Cu_3O_{6+y}$ (YBCO) system (including bilayer CuO_2 planes and uniaxial CuO chain layer) in the superconducting state. We show that the observed in-plane anisotropy in the spin-excitation spectrum of YBCO – which is often interpreted as an evidence for the electron nematic phase – can alternatively be explained via incorporating the uniaxial CuO chain's contribution. We demonstrate that the neutron spectra in YBCO is dominated by the contribution from the four-fold symmetric CuO_2 plane state as in other cuprates, however, it acquires an in-plane anisotropy via finite interlayer coupling with the chain state. The result rules out the claim that an electronic nematic phase is responsible for the pseudogap state in YBCO.

PACS numbers: 71.10.Hf,73.43.Nq,74.40.Kb,74.72.Kf

I. INTRODUCTION

The formation of electronic liquid crystals is intimately related to two-dimensional anisotropy phenomena, which are of intense current interests in the field of strongly correlated electrons, semiconductors,[1] 2D electron gas,[2] graphene[3] as well as in cold atom systems.[4] The surge of interests has recently been extended to various families of unconventional superconductors including cuprates,[5–9] pnictides,[10] $Sr_3Ru_2O_7$,[11] and heavy fermion URu_2Si_2.[12,13] The microscopic origin for the in-plane anisotropy in these superconducting (SC) systems which consistently accommodate tetragonal crystal symmetry is more interesting and exotic. A general question that underlies all these materials is whether the anisotropic structure is related to an emergent nematic electronic liquid crystal phase or merely comes from the subtle crystallographic distortion or something else.

In cuprates, pnictides, and heavy fermion URu_2Si_2[12,13] systems, this question has posed widespread research interests with the hope to explain their unusual normal state phases from which the SC state is arguably derived. In cuprates, the experimental evidences of the in-plane anisotropy have been taken seriously as a definite evidence for the presence of the electronic crystal liquid phase,[18,21] and also been extended to explain the so-called 1/8 doping problem where superconductivity is strongly quenched.[22] Here we provide a different mechanism for the origin of the in-plane anisotropy in $YBa_2Cu_3O_{6+y}$ (YBCO). We demonstrate that, even in the absence of any crystal anisotropy or 'nematic' ground state, an anisotropy is introduced to the SC CuO_2 plane state via the interlayer electronic coupling with the quasi-1D CuO chain bands.

Experimental implications of anisotropy in cuprates: The CuO_2 plane state is present in all cuprates, and is arguably responsible for most of the exotic low-energy phases which vary dramatically within the same family. A stripe-like modulation has been well established in $La_{2-x}(Sr/Ba)_xCuO_4$ (LS/BCO),[23] $Bi_2Sr_2CaCuO_{8+\delta}$ (BSCCO)[24], $Ca_{2-x}Na_xCuO_2Cl_2$,[25] and $HgBa_2CuO_{4+\delta}$ (HBCO)[26]. On the other hand, most evidences for the anisotropic structure have been obtained in YBCO via transport,[5] Nernst,[9] and inelastic neutron scattering (INS) measurements[6], with some recent indication of this phase in BSCCO from scanning tunneling microscopy (STM).[7,8] This material variant pseudogap properties raise an essential question: *Is the mechanism of pseudogap different in different cuprates, or such differences merely arise from the material dependent electronic structure?* By closely looking at the YBCO crystal, we indeed notice that this system hosts both

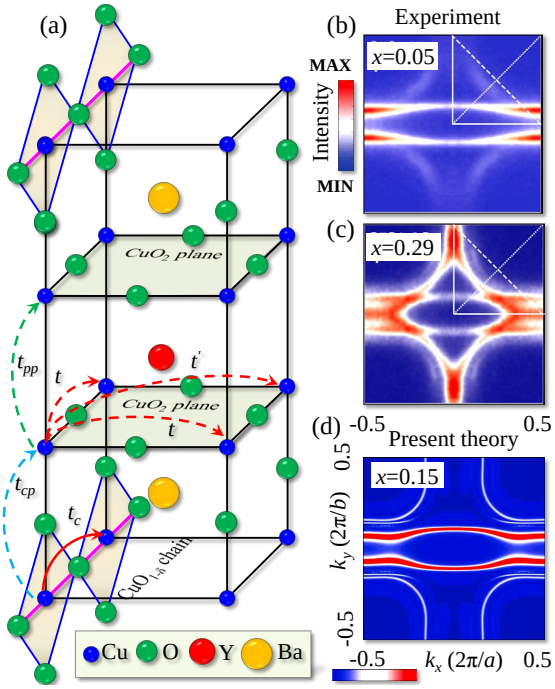

FIG. 1. (Color online) (a) Crystal structure of YBCO with two CuO chain layers residing at the top and bottom of the unit cell, and two CuO_2 planes intervening between them. Arrows dictate all the electronic hoppings considered in this calculation (except t'' which is not shown). (b)-(c) ARPES results of FS in the extreme underdoping and overdoping region of YBCO sample.[31] Here x is the hole doping, not the oxygen content. (d) Computed FS in the paramagnetic state near the optimal doping region. The spectral weight is most dominant on the chain band, while the bi-layer splitting in the CuO_2 bands is hardly visible, due to spectral weight distribution among the tri-layers.

quasi-2D CuO_2 layers and quasi-1D CuO chain layers, as shown in Fig. 1(a). The FSs measured by angle-resolved photoemission spectroscopy (ARPES) in the underdoped [Fig. 1(b)] and overdoped [Fig. 1(c)] region exhibit that while a pseudogap is opened in the CuO_2 bi-layer bands, but the 1D CuO chain FS remains ungapped at all finite dopings.[28,31] Additionally, a visual estimation to the Fermi arc seen in the underdoped case does not reveal any significant presence of four-fold symmetry breaking, thus indicating that the origin of pseudogap is not directly related to the observed anisotropy in this system. On the other hand, YBCO being a polar compound, there exists a charge transfer between the layers as a result of the electric fields generated by the polar unit cell.[27] We compute the INS spectra by realistic multi-layer BCS-RPA calculation to demonstrate that the interlayer coupling between the chain and plane layers stipulates a two-fold symmetry in the electronic states even when the isolated bulk planer states do not intrinsically involve any spontaneous four-fold symmetry breaking.

The rest of the paper is organized as follows. In Sec. II, we introduce the tight-binding model for the trilayer YBCO system and the corresponding multi-layer spin-excitation calculation. The results for the static spin-susceptibility at zero energy and the role of two plane FS as and the chain FS are given in Sec. III. In the SC state, the origin of the in-plane anisotropy in the dynamical spin-excitation spectrum is demonstrated in Sec. IV. The doping and energy dependence of the FS nesting and the in-plane anisotropy is calculated and discussed in the context of YBCO phase diagram in Sec. V. Finally we discuss and conclude in Sec. VI.

II. TIGHT-BINDING MODEL

To realistically model the low-lying electronic states of YBCO, one requires a minimum of three band model to incorporate the bi-layer splitting and the chain band, coming from CuO_2-CuO_2-CuO trilayers.[30] In each isolated layer, the single electron hopping between Cu $d_{x^2-y^2}$ orbitals is mediated by O atoms, which is captured by effective tight-binding hopping parameters. For the plane and chain layers, it is sufficient to consider up to third and next nearest neighbor hoppings, respectively [see Fig. 1(a)], which construct the isolated layer dispersions $\xi_{(p/c)\boldsymbol{k}}$ as[32]

$$\xi_{p\boldsymbol{k}} = -2t(c_x + c_y) - 4t' c_x c_y - 2t''(c_{2x} + c_{2y}) - \mu_p, \quad (1)$$

$$\xi_{c\boldsymbol{k}} = -2t_c c_y - \mu_c. \quad (2)$$

Here $c_{\alpha x/y} = \cos(\alpha k_{x/y} a)$ and $\mu_{c/p}$ are the chemical potentials for the plane and chain bands, which encode the onsite potential imbalance and other crystal field effects between the two layers. We consider the interlayer coupling within single electron tunneling matrix-element t_{pp} and t_{cp}, which obey periodic boundary condition along the c-axis. Therefore the final Hamiltonian in the trilayer basis is,

$$H_{\boldsymbol{k}} = \begin{pmatrix} \xi_{p\boldsymbol{k}} & t_{pp} & t_{cp} \\ t_{pp} & \xi_{p\boldsymbol{k}} & t_{cp} \\ t_{cp} & t_{cp} & \xi_{c\boldsymbol{k}} \end{pmatrix}. \quad (3)$$

Note that while isolated plane dispersion $\xi_{p\boldsymbol{k}}$ obeys four-fond symmetry, the total Hamiltonian in Eq. 3 breaks this symmetry due to its coupling with the chain band via t_{cp}. In other words, all eigenvalues and eigenstates including that for the plane states are two-fold symmetric. The computed spectral weight function on the 2D momentum space at the Fermi level is plotted in Fig. 1(d) at a representative doping $x = 0.15$ [this choice of doping represents $YBCO_{6.45}$ at which the neutron scattering data is compared below], which agrees well with the corresponding FS trend obtained in ARPES data [Figs. 1(b)-(c)].[31]

A. Multilayer BCS susceptibility

The superconductivity is taken to be d-wave like for all three bands, where the value of the SC gap amplitude is constrained by the experimental value[31,33] of Δ =34 meV.[34] In the SC state, the layer-dependent BCS spin-susceptibility tensor is computed from

$$\chi^{jj'0}_{ii'}(\boldsymbol{q}, i\omega_m) = -\frac{1}{4N} \sum_{\boldsymbol{k},n,\nu,\nu'} M^{\nu,\nu'}_{ii'jj'}(\boldsymbol{k}, \boldsymbol{q}) \\ \mathrm{Tr}\left[G^{\nu}(\boldsymbol{k}, i\Omega_n) G^{\nu'}(\boldsymbol{k}+\boldsymbol{q}, i\Omega_n + i\omega_m) \right]. \quad (4)$$

For each band, G is the 2×2 Green's function, made of normal and anomalous parts in the Nambu-Gorkov's notation.[35] The interlayer coupling matrix element is $M^{\nu,\nu'}_{ii'jj'}(\boldsymbol{k}, \boldsymbol{q}) = \phi^{i}_{\nu}(\boldsymbol{k}) \phi^{j\dagger}_{\nu}(\boldsymbol{k}) \phi^{i'}_{\nu'}(\boldsymbol{k}+\boldsymbol{q}) \phi^{j'\dagger}_{\nu'}(\boldsymbol{k}+\boldsymbol{q})$, where $\phi^{i}_{\nu}(\boldsymbol{k})$ is the eigenstate of band ν or layer i. In this notation, ν (ν') is the initial (final) eigenstate, consists of hybridization between i and j (i' and j') layers, and ϕ is the corresponding eigenvector.

RPA:- Finally, we incorporate the many-body interaction within random-phase approximation (RPA) as $\tilde{\chi}(\boldsymbol{q}, \Omega) = \tilde{\chi}(\boldsymbol{q}, \Omega)[\mathbf{1} - \tilde{U}\tilde{\chi}(\boldsymbol{q}, \Omega)]^{-1}$ (the symbol tilde represents tensor). Since, we consider only the $d_{x^2-y^2}$-orbital for all three layers, no inter-orbital couplings such as Hund's coupling are involved here. We include intra-layer interaction for plane and chain as U_p and U_c, respectively and the inter-layer one between plane-plane and chain-plane layers as U_{pp} and U_{cp}.[43]

III. ANISOTROPY IN STATIC SUSCEPTIBILITY AND THE ROLE OF FS NESTING

Figure 2 shows the relevant components of the static RPA susceptibilities in the normal state and their corresponding FS nestings. The intraplaner component, in Fig. 2(a), obtains a leading incommensurate nesting at $\boldsymbol{q}^{pp}_a = (\pi(1-\delta_a), \pi)$ and $\boldsymbol{q}^{pp}_b = (\pi, \pi(1-\delta_b))$, where δ_a and δ_b measure the degree of incommensurability along a and b bond directions. Comparing these two nesting peaks, we immediately find that there is a prominent anisotropy present in both intensity and magnitude of δ_a and δ_b. The origin of this anisotropy can be traced back to the FS anisotropy of the plane band shown by blue lines in Fig. 2(e). This anisotropy in the plane state is introduced via its hybridization with the chain layer (recall that the

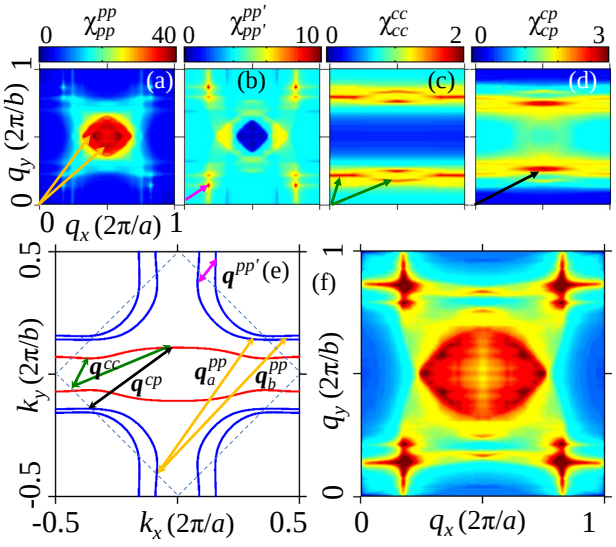

FIG. 2. (Color online) (a)-(d) Various representative components of the static RPA susceptibility in the normal state at x=0.15. The dominant nesting in each component is depicted by arrows. The arrows of same color are overlayed on the corresponding FS in (e). (e) The FS obtained from Fig. 1(d). (f) Total RPA susceptibility (summing over all components).

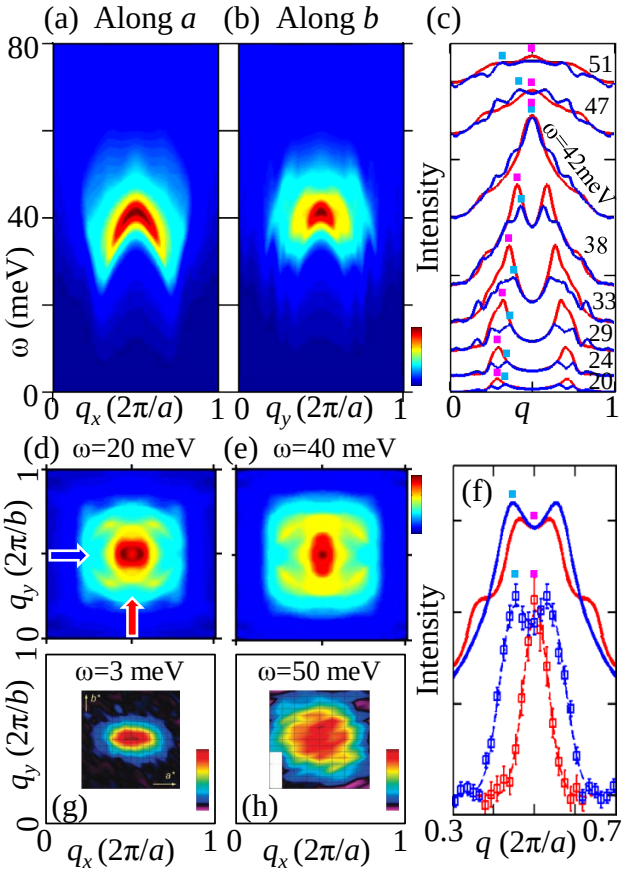

FIG. 3. (Color online) (a)-(b) Computed imaginary part of the total susceptibility, χ'', in the SC state plotted along $(0,\pi) \rightarrow (2\pi,\pi)$ in (a), and $(\pi,0) \rightarrow (\pi,2\pi)$ in (b) (a- and b-bond directions, respectively). (c) Several representative constant energy cuts of χ'' are shown as a function of $\boldsymbol{q}$ along a- and b-bond directions. Each spectra are shifted vertically by a constant value for visualization. The peak position of each spectrum is marked by a small vertical line. (d)-(e) Two representative constant energy profiles of χ'' shown below and near the resonance, respectively. (f) Two representative momenta cuts through (e) (arrows) shown near Q, and compared with corresponding experimental data (symbols of same color).[6] The intensities of the theoretical and experimental data are normalized arbitrarily to ease the comparison. The dashed line through the experimental data is a guide to the eye. (g)-(h) The constant energy experimental profiles .[6]

isolated plane dispersion, $\xi_{p\boldsymbol{k}}$, itself obeys four-fold symmetry). The bi-layer splitting in the plane bands is clearly visible near $\boldsymbol{k} = (0, \pm\pi)$ points while near $\boldsymbol{k} = (\pm\pi, 0)$, it mixes with the chain bands. The nesting between these split bands, $\boldsymbol{q}^{pp'}$, produces a susceptibility peak in the vicinity of $\mathbf{q} \sim \Gamma$, as seen in Fig. 2(b). The intra-chain and chain-plane components of the susceptibility in Figs. 2(c) and 2(d), respectively are naturally dominated by the quasi-1D components. Summing over its components at each $\boldsymbol{q}$ and ω, we see that the full susceptibility accommodates the coexistence of several nestings with relative intensities, see Fig. 2(f). The competition between various instabilities originating from the leading nesting is strongly doping dependent, and hence on the FS topological changes as discussed below in Fig. 4.

IV. ANISOTROPY IN SPIN RESONANCE AND SUPERCONDUCTIVITY

INS directly measures the imaginary part of the spin susceptibility as a function of $\mathbf{q}$ and ω. Within the standard itinerant picture of unconventional superconductivity, a spin resonance develops in the SC state due to the sign-reversal of the SC order parameters at the FS nesting vectors.[36,37] On the basis of this theory, only $\boldsymbol{q}^{pp}$ vector contributes to the BCS susceptibility, while the other nesting vectors disappear or become suppressed in the SC state (of course, the inelastic scattering activates other possible scattering channels, however, their intensities are shown earlier to be comparatively less[37]). The computed spin resonance spectra plotted along a- and b-bond directions in Figs. 2(a) and 2(b), respectively, reveal that the anisotropy between δ_a, δ_b acquires energy dependence due to the d-wave nature of the SC gap. At zero energy, both $\boldsymbol{q}_{a/b}^{pp}$ touches the nodal points, where $\delta_{a/b}$ attain their maximum amplitudes. With increasing energy, $\boldsymbol{q}_{a/b}^{pp}$ approach towards $\boldsymbol{Q}$, and thereby reducing the values of $\delta_{a/b}$. Finally, at $\omega = 40$ eV, both $q_{a/b}^{pp}$ march at $\boldsymbol{Q} = (\pi,\pi)$, the intensity of χ'' becomes maximum and a resonance peak appears. Although the anisotropy disappears at the resonance in its magnitude ($\delta_a = \delta_b = 0$), but it remains present in the intensity as can be seen from Fig. 2(e), due to overlap matrix-element effect between plane and chain layers, see Eq. 4. In fact, the anisotropy becomes reversed at and above the resonance energy, as demonstrated in Fig. 3(c). The results agree well with the experimental data of $YBCO_{4.5}$, presented in Figs. 2(f)-

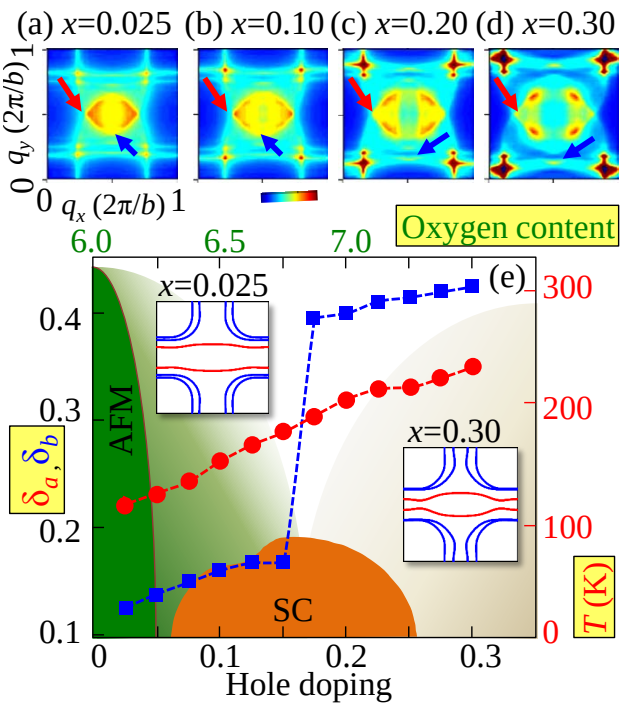

FIG. 4. (Color online) (a)-(d) Static susceptibility at $\omega = 0$ plotted at four representative dopings. The evolution of the dominating nesting from the vicinity of Q [arrow in (a)] towards the chain band near $(\pi/2, 0)$ [arrow in (d)] as a function of doping is clearly visible. (e) The degree of incommensurability along a and b axes, defined in text by δ_a and δ_b, respectively is shown as a function of doping. The interesting jump in the value of δ_b at $x = 0.15$ is associated with the shift of spectral weight from the plane layer to the chain layer (see text). Different color shadings represent standard YBCO phase diagram.[28,33] *Insets:* Computed FSs at two extreme dopings of YBCO.

2(h); the difference in the energy scale between Figs. 3(d) and 3(g) notwithstanding.

V. DOPING DEPENDENCE OF ANISOTROPY

Finally, we study the doping evolution of the anisotropy in YBCO, and compare it with the YBCO phase diagram in Fig. 4. In the extreme underdoped region $x = 0.025$, the leading static instability in $\chi'(\mathbf{q}, \omega = 0)$ commences at $\boldsymbol{q}^{pp}$ with both the magnitude and intensity of δ_a being larger than those of δ_b, as seen in Fig. 4(a). With increasing doping, we notice several interesting characteristic evolution of the susceptibility: (1) Both δ_a and δ_b increase almost monotonically with doping, however the degree of anisotropy or the difference $\delta_a - \delta_b$, does not have significant doping dependence upto $x \sim 0.15$, see Fig. 4(e). (2) With further hole doping, the incommensurate peaks along the bond directions $\boldsymbol{q}_a^{pp}$ and $\boldsymbol{q}_b^{pp}$ begin to split. Above x=0.15, the splitting becomes sufficiently large so that the maximum intensity in the vicinity of $\boldsymbol{Q}$ does not remain aligned along the bond directions, but rotates by 45^0 to the diagonal directions [see Figs. 4(c)-(d)]. It is noteworthy that the 45^o of the INS spectra as a function of doping is observed earlier in La-based materials where such rotation occurs at the beginning of the SC dome around x=0.05,[38] while in the present case of YBCO, this crossover doping coincides with the optimal doping of this compound. (3) The doping gradually increases intensity at other small nesting vectors $\boldsymbol{q}^{pp'/cc}$ near Γ point, which all participate in nesting the van-hove singularity (VHS) region of the quasi-2D plane bands, and the quasi-1D FSs of the chain bands, respectively, as defined in Fig. 2(e). With hole doping, these flat FSs move towards each other [compare FSs at x=0.025 and x=0.30 in the *insets* to Fig. 4(e)], and thereby enhance nestings. Similar VHS nesting has been theoretically predicted to be present in the single-layer BSCCO band structure,[39] and observed in the quasiparticle interference (QPI) pattern of the same compound as probed by STM[40] (in YBCO, this nesting additionally breaks four-fold symmetry). However, as mentioned earlier, these nestings do not survive in the SC state, because they do not involve sign-reversal of the d-wave SC gap, and thus can not be detected by INS. (4) Above the optimal doping, the maximum intensity at δ_b jumps suddenly from the (π, π) region (plane bands) to the chain band region at $\boldsymbol{q}^{cp}$ [dictated by arrows in Figs. 4(d) and 2(e)] as plotted by square symbols in Fig. 4(e). As the chain band is 1D, $\boldsymbol{q}^{cp}$ only appears along 1D, while the incommensurate peak along the a-bond direction continues to be dominated by plane states. This is why, the anisotropy between δ_a and δ_b becomes reversed above the optimal doping.

VI. DISCUSSION AND CONCLUSION

Does anisotropy cause nematic pseudogap order? Coincidentally, the crossover of the leading instability from the plane to the chain band occurs at the doping where evidences are mounting in YBCO that the pseudogap also disappears.[26,28,33] On the basis of these results as well as numerous evidences for the presence of FS reconstruction in the pseudogap region of YBCO, we conjecture that if pseudogap arises from a FS nesting, the planer nesting $\boldsymbol{q}^{pp} \sim (\pi, \pi)$ that dominates in this doping region, is most likely be the one.[20,41] The leading nesting at $\boldsymbol{q}^{pp}$ also prohibits the possibility of stabilizing a charge density wave (CDW) in the 1D chain bands via Peierls instability at $\boldsymbol{q}^{cc/cp}$ in the pseudogap state. CDW can at most be present as a secondary order.[44] Recalling the ARPES results presented in Fig. 1(b)-(c), our results are consistent with the observed ungapped chain bands at all finite dopings.

Conclusions:- In summary, we provide a microscopic model for the trilayer YBCO superconductor to explain the observed in-plane anisotropy in the spin-excitation spectrum of this compound. We calculate multi-layer BCS susceptibility within RPA formalism to show that while the isolated planer electronic states intrinsically obey four-fold rotational symmetry, but its observables exhibit a reduced two-fold symmetry due to inter-layer coupling with the quasi-1D chain bands. The computed INS spectra exhibit considerable anisotropy in its incommensurate structure which varies with energy upto the resonance energy scale, in quantitative agree-

ment with experimental data at the same doping. We also present verifiable prediction that the anisotropy becomes reversed above optimal doping in YBCO. We conclude that an incommensurate order with planer nesting around (π, π) is the leading nesting as in other cuprates, while the anisotropy is a secondary effect coming form the chain state. Our results rule out the earlier postulate that nematic order may be the origin of pseudogap phase in YBCO.

ACKNOWLEDGMENTS

The work is supported by the U.S. DOE through the Office of Science (BES) and the LDRD Program and facilitated by NERSC computing allocation.

[1] K. B. Cooper, M. P. Lilly, J. P. Eisenstein, L. N. Pfeiffer, K. W. West, Phys. Rev. B **65**, 241313 (2002).

[2] M. P. Lilly, K. B. Cooper, J. P. Eisenstein, L. N. Pfeiffer, K. W. West, Phys. Rev. Lett. **82**, 394 (1999).

[3] A. S. Mayorov, D. C. Elias, M. Mucha-Kruczynski, R. V. Gorbachev, T. Tudorovskiy, A. Zhukov, S. V. Morozov, . M. I. Katsnelson, V. I. Falako, A. K. Geim, K. S. Novoselov, Science **333**, 860 (2011).

[4] A. F. Ho, M. A. Cazalilla, and T. Giamarchi, Phys. Rev. Lett. **92**, 130405 (2004).

[5] Y. Ando, K. Segawa, S. Komiya, and A. Lavrov, Phys. Rev. Lett. **88**, 137005 (2002).

[6] V. Hinkov, D. Haug, B. Fauque, P. Bourges, Y. Sidis, A. Ivanov, C. Bernhard, C. T. Lin, B. Keimer, Science **319**, 597 (2008).

[7] A. Mesaros, K. Fujita, H. Eisaki, S. Uchida, J. C. Davis, S. Sachdev, J. Zaanen, M. J. Lawler, Eun-Ah Kim, Science **333**, 426 (2011).

[8] M. J. Lawler, K. Fujita, J. Lee, A. R. Schmidt, Y. Kohsaka, C. Koo Kim, H. Eisaki, S. Uchida, J. C. Davis, J. P. Sethna, and Eun-Ah Kim, Nature **466**, 347 (2010).

[9] R. Daou, J. Chang, D. Leboeuf, O. Cyr-Choini'ere, F. Laliberte, N. Doiron-Leyraud, B. J. Ramshaw, R. Liang, D. A. Bonn, W. N. Hardy, and L. Taillefer, Nature **463**, 519 (2010); J. Chang, N. Doiron-Leyraud, F. Laliberte, R. Daou, D. LeBoeuf, B. J. Ramshaw, R. Liang, D. A. Bonn, W. N. Hardy, C. Proust, I. Sheikin, K. Behnia, and L. Taillefer, Phys. Rev. B **84**, 014507 (2011);

[10] T.-M. Chuang, M. P. Allan, J. Lee, Y. Xie, Ni Ni, S. L. Budko, G. S. Boebinger2, P. C. Canfield, and J. C. Davis, Science **327**, 181 (2010).

[11] R. A. Borzi, S. A. Grigera, J. Farrell, R. S. Perry, S. J. S. Lister, S. L. Lee, D. A. Tennant, Y. Maeno, A. P. Mackenzie, Science **315**, 214 (2007).

[12] R. Okazaki, T. Shibauchi, H. J. Shi, Y. Haga, T. D. Matsuda, E. Yamamoto, Y. Onuki, H. Ikeda, and Y. Matsuda, Science **331**, 439 (2011).

[13] Tanmoy Das, arXiv: 1201.2246.

[14] In YBCO, it is observed that a nematic phase forms around T $\sim$150 K (YBCO),[6] which is higher than the 'pseudogap' temperature T^* $\sim$200 K for this compound,[33,42] and also higher than the onset of orthorombic distortion or the low-temperature orthorombic phase in LSCO[23] and in pnictide [J.-H. Chu, Science **329**, 824 (2010)].

[15] M. Vojta, T. Vojta, and R. K. Kaul, Phys. Rev. Lett. **97**, 097001 (2006); J. Wang, G.-Z. Liu, and H. Kleinert, Phys. Rev. B **83**, 214503 (2011); M. Vojta, Eur. Phys. J. Special Topics **188**, 49 (2010).

[16] S. Okamoto, D. Sénéchal, M. Civelli, A.-M. S. Tremblay, Phys. Rev. B **82**, 180511(R) (2010).

[17] Y. Furukawa, T. Ohashi, Y. Koyama, and N. Kawakami, Phys. Rev. B **82**, 161101(R) (2010).

[18] C. Pépin, M. R. Norman, S. Burdin, and A. Ferraz, Phys. Rev. Lett. **106**, 106601 (2011).

[19] M. Capati, M. Grilli, and J. Lorenzana, arXiv:1106.3238.

[20] A. J. Millis and M. R. Norman, Phys. Rev. B **76**, 220503 (2007); Q. Luo, D.-X. Yao, A. Moreo, and E. Dagotto, Phys. Rev. B **83**, 174513 (2011).

[21] S. A. Kivelson, I. P. Bindloss, E. Fradkin, V. Oganesyan, J. M. Tranquada, A. Kapitulnik and C. Howald, Rev. Mod. Phys. **75**, 1201 (2003); H. Yao, D.-H. Lee, and S. Kivelson, Phys. Rev. B **84**, 012507 (2011).

[22] G.-Z. Liu, J.-R. Wang, and J. Wang, arXiv:1111.1686.

[23] J. Tranquada, H. Woo, T. Perring, H. Goka, G. Gu, G. Xu, M. Fujita, and K. Yamada, Nature **429**, 534 (2004).

[24] C. V. Parker, P. Aynajian, E. H. da Silva Neto, A. Pushp, S. Ono, J. Wen, Z. Xu, G. Gu, and A. Yazdani Nature **468**, 677 (2010).

[25] K. M. Shen, F. Ronning, D. H. Lu, F. Baumberger, N. J. C. Ingle, W. S. Lee, W. Meevasana, Y. Kohsaka, M. Azuma, M. Takano, H. Takagi and Z.-X. Shen, Science **307**, 901 (2005).

[26] Y. Li, V. Balédent, N. Barisc, Y. Cho, B. Fauque, Y. Sidis, G. Yu, X. Zhao, P. Bourges, and M. Greven, Nature **455**, 372 (2008).

[27] It is known that YBCO crystals mostly cleave between the CuO chain and the BaO layers, exposing the CuO chain to the surface.[28]

[28] M.A. Hossain, J.D.F. Mottershead, A. Bostwick, J.L. McChesney, E. Rotenberg, R. Liang, W.N. Hardy, G.A. Sawatzky, I.S. Elfimov, D.A. Bonn, A. Damascelli, Nature Physics **4**, 527 (2008).

[29] G. Grüner, Density waves in solids, Addison-Wesley, Reading, MA, 1994.

[30] W. A. Atkinson, Phys. Rev. B **59**, 3377 (1999).

[31] D. Fournier, G. Levy, Y. Pennec, J.L. McChesney, A. Bostwick, E. Rotenberg, R. Liang, W.N. Hardy, D.A. Bonn, I.S. Elfimov, A. Damascelli, Nature Physics **6**, 905 (2010) .

[32] The parameters are obtained after fitting to the experimental FS[30] as $(t, t', t'', t_c, t_{pp}, t_{cp}, \mu_p, \mu_c)$=(600,-120,150,400,400,600,-10,-600) in meV. The doping is calculated within a standard rigid band shift approximation.

[33] S. Huefner, M.A. Hossain, A. Damascelli, G.A. Sawatzky, Rep. Prog. Phys. **71**, 062501 (2008).

[34] The widely used proximity model for YBCO suggests that the d-wave superconductivity is induced to the chain layer from the plane one due to interlayer coupling [D. K. Morr and A. V. Balatsky, Phys. Rev. Lett. **87**, 247002 (2001)]. We take the gap amplitude to be same for all bands to reduce the number of parameters.

[35] The components of the BCS Green's function are $G^{\nu}_{11/22}(\boldsymbol{k}, i\omega_n) = (i\omega_n + \xi_{\nu\boldsymbol{k}})/(\omega_n^2 + E^2_{\nu\boldsymbol{k}})$ and $G^{\nu}_{12}(\boldsymbol{k}, i\omega_n) = G^{\nu *}_{21}(\boldsymbol{k}, i\omega_n) = \Delta_{\nu\boldsymbol{k}}/(\omega_n^2 + E^2_{\nu\boldsymbol{k}})$, where the SC quasiparticles are $E_{\nu\boldsymbol{k}} = \pm\sqrt{\xi^2_{\nu\boldsymbol{k}} + \Delta^2_{\nu\boldsymbol{k}}}$. ($G_{12}$ is sometimes denoted by F.) We perform Matsubara frequency

summation over the fermionic index n, while the bosonic Matsubara frequency is treated by taking analytical continuation to the real axis as $i\omega_m = \omega + i\delta$ (δ is small broadening).

[36] T. Das and A. V. Balatsky, Phys. Rev. Lett. **106**, 157004 (2011); *ibid* Phys. Rev. B **84**, 014521 (2011); and the references therein.

[37] T. Das, R. S. Markiewicz, and A. Bansil, Phys. Rev. B **85**, 064510 (2012).

[38] K. Yamada, C. H. Lee, K. Kurahashi, J. Wada, S. Wakimoto, S. Ueki, H. Kimura, Y. Endoh, S. Hosoya, G. Shiranem R. J. Birgeneau, M. Greven, M. A. Kastner, and Y. J. Kim, Phys. Rev. B **57**, 6165 (1998).

[39] R. S. Markiewicz, J. Lorenzana, and G. Seibold, Phys. Rev. B **81**, 014510 (2010).

[40] W. D. Wise, K. Chatterjee, M. C. Boyer, T. Kondo, T. Takeuchi, H. Ikuta, Z. Xu, J. Wen, G. D. Gu, Y. Wang, and E. W. Hudson, Nature Physics **5**, 213 (2009).

[41] A. Hackl, M. Vojta, and S. Sachdev, Phys. Rev. B **81**, 045102 (2010); N. Harrison, and S. E. Sebastian, Phys. Rev. Lett. **106**, 226402 (2011).

[42] H. A. Mook, P. Dai, S. M. Hayden, A. Hiess, S-H Lee, and F. Dogan, Phys. Rev. B **69**, 134509 (2004).

[43] Denoting the intra-layer interactions for plane and chain as U_p and U_c, respectively and the inter-layer one between plane-plane and chain-plane layers as U_{pp} and U_{cp}, the nonvanishing components of the $\tilde{U}$ tensor are $\tilde{U}^{ii}_{ii} = U_i$, $\tilde{U}^{ij}_{ij} = U_{ij}$ (where $i, j = p, c$). The values of each components of $\tilde{U}$ are constrained by their corresponding components of $\tilde{\chi}$ to avoid an instability, see Fig. 2, and the obtained values are $(U_p, U_c, U_{pp}, U_{cp})$=(3,2,0.5,0.4) in eV.

[44] V. B. Zabolotnyy, V. B. Zabolotnyy, A. A. Kordyuk, D. Evtushinsky, V. N. Strocov, L. Patthey, T. Schmitt, D. Haug, C. T. Lin, V. Hinkov, B. Keimer, B. Bchner, S. V. Borisenko, Phys. Rev. B **85**, 064507 (2012).